Diffraction diagnosis of protein folding in gap junction connexons

Thomas T. Tibbitts, D. L. D. Caspar, W. C. Phillips, and D. A. Goodenough*
Rosenstiel Basic Medical Sciences Research Center, Brandeis University, Waltham, Massachusetts 02254-9110; and
*Department of Anatomy and Cellular Biology, Harvard Medical School, Boston, Massachusetts 02115 USA

ABSTRACT To diagnose the regular polypeptide conformation in gap junction membranes, the x-ray intensities diffracted from oriented specimens have been separated into a modulated component due to the coherently ordered portion of the channel-forming pairs of connexon hexamers and a diffuse component due to the disordered parts. The spherically averaged ordered protein diffraction, in the resolution range 15–4 Å, was compared with intensity curves calculated from the Fourier transforms of proteins representive of the major tertiary structural classes. From this comparison the α-helical content of the ordered portion of the connexon was estimated to be ~60%. Calculation of cylindrically averaged patterns for oriented distributions of α-helical and β-sheet proteins demonstrated that the ratio of the modulated diffracted intensity near 5 Å spacing on the meridian and 10 Å spacing on the equator observed from the gap junctions can be accounted for by α-helical segments inclined relative to the connexon axis. Model dimers of connexonlike hexamers were constructed from α-helix bundle proteins to correlate features in the calculated diffraction patterns with the model parameters. On the basis of these correlations, the ordered gap junction diffraction data indicate that α-helical segments centered at 38 Å from the midplane of the gap have a mean radial location ~24 Å from the hexamer axis, and an axial projected length of ~35 Å. Thus, these α-helical segments traverse the hydrocarbon core of the lipid bilayer, as expected for the four hydrophobic sequences of the connexin molecule.

INTRODUCTION

The connexon hexamers, which pair together in gap junction membranes to form channels for intercellular communication, have been structurally characterized at ~25 Å resolution by x-ray diffraction (Makowski et al., 1977, 1984*b*) and electron microscopy studies (Unwin and Zampighi, 1980; Unwin and Ennis, 1984) of specimens isolated from rat and mouse livers. Amino acid sequences for the related connexin molecules of gap junctions from various tissues and species have been determined by recombinant DNA methods (Paul, 1986; Kumar and Gilula, 1986; Beyer et al., 1987; Gimlich et al., 1988); and distinctive hydrophobic sequences have been identified as α-helical transmembrane segments (Unwin, 1986; Hertzberg et al., 1988; Milks et al., 1988). X-Ray diffraction data in the 10 Å and 5 Å spacing regions have been respectively taken as indicating α-helical (Makowski et al., 1977) or β-sheet structures (Makowski et al., 1982) within the membrane bilayer. The α- and β-polypeptide conformations were first identified in fibrous proteins from their characteristic x-ray patterns (Astbury and Street, 1931) before the α-helix and β-sheet structures were discovered by Pauling and Corey (1951*a* and *b*). Since the α- and β-conformations diffract distinctively, it should be possible to diagnose the dominant folding of the connexin molecules from the gap junction diffraction data.

X-Ray crystallography has provided atomic resolution pictures of the arrangement of α-helices and β-sheets in a wide variety of crystalline proteins (*cf.* Richardson, 1981); and spectroscopic methods have been devised to assess the proportions of these conformations in noncrystalline states (*cf.* Cantor and Schimmel, 1980). But, beyond the pioneering studies on fibrous proteins, there have been only limited applications of diffraction methods to diagnose secondary structure in noncrystalline proteins. Diffraction patterns from oriented one- and two-dimensionally periodic protein assemblies provide significant information about the type and orientation of the secondary structural elements in the constituent molecules. For example, the α-helical coiled-coil conformation of the filamentous bacteriophage coat protein was identified from the high angle x-ray fiber pattern (Marvin, 1966) before the symmetry and subunit packing arrangement were established from the lower resolution diffraction data (Makowski et al., 1980; Marvin, et al.; 1981); and the number and orientation of the α-helical segments in bacteriorhodopsin were inferred from the intensity distribution of the equatorial diffraction from stacked

Dr. Tibbitts' present address is Center for Molecular Biophysics, Boston University Department of Physics, 590 Commonwealth Ave., Boston, MA 02215.

purple membrane (Henderson, 1975) before these segments were visualized by electron microscopy (Henderson and Unwin, 1975). Our goal in this paper is to develop systematic methods for evaluating 15–4 Å resolution diffraction data from noncrystalline protein assemblies to characterize the secondary structure in gap junction membranes.

In an early study on noncrystalline specimens, Riley and Arndt (1953) showed that a variety of unoriented, dried proteins gave similar x-ray powder patterns with diffraction maxima near 10 and 4.5 Å spacing. Their results indicated that the spherically averaged distribution of interatomic vectors of length <6 Å was relatively invariant in the proteins they compared, including native and denatured serum albumin, but the strength of the ~10 Å periodicity in the different structures was variable. By comparison of the spherically averaged diffraction data for crystals representative of the four classes of globular protein tertiary structure, Richardson and Richardson (1985) demonstrated that the intensity of the peak near 10 Å spacing relative to that near 4.5 Å spacing was stronger in the patterns from proteins with high α-helical content. To quantify and extend this criterion for diagnosis of protein folding, we have calculated spherically and cylindrically averaged diffraction patterns from the Fourier transforms of representative structural types of well-characterized crystalline proteins. Furthermore, cylindrically averaged diffraction patterns of imperfectly oriented assemblies of some of these proteins have been calculated for comparison with diffraction data from stacked gap junction membranes.

The angular spread for the best oriented gap junction specimens is $\sim\pm 15°$, which smears details in the diffraction patterns. The dominant diffraction features related to secondary structure are an equatorial arc centered at ~11 Å spacing, with an angular width somewhat greater than the orientation distribution, and a set of meridional fringes, with even wider angular spread, centered at ~4.9 Å spacing. The equatorial diffraction was initially interpreted as due to transmembrane α-helices (Makowski et al., 1977); but, because α-helices perpendicular to the membrane plane would not account for the meridional intensity maxima, the high-angle pattern was later taken to signify a cross-β conformation (Makowski et al., 1982; Caspar et al., 1988). Evidence regarding the folding of the gap junction protein has been obtained from hydrophobicity plots of connexin amino acid sequences (Paul, 1986; Kumar and Gilula, 1986) and maps of the transmembrane topology deduced from antibody binding and proteolytic susceptibility studies (Hertzberg et al., 1988; Milks et al., 1988; Goodenough et al., 1988). Interpretations of these data have led to the inference that there are four α-helical segments spanning the membrane bilayer (Unwin, 1986; Hertzberg et al., 1988; Milks et al., 1988). Our quantitative comparison of gap junction diffraction data with patterns calculated from the transforms of proteins of known structure supports the α-helical model and indicates the location and range of tilts of the transmembrane helices relative to the axis of the connexon hexamer. Comparison of model diffraction patterns with experimental data to determine the length, location, and tilt of the helix segments has depended upon the development of an efficient numerical method for computing patterns for imperfectly oriented models built with different arrangements of secondary structural elements.

METHODS

Specimen preparation and data processing

Preparation of gap junction membranes from rodent liver involved isolation of a plasma membrane fraction in low ionic strength bicarbonate buffer, followed by detergent treatment (Fallon and Goodenough, 1981). Plaques were stacked by centrifugation and partial dehydration to form oriented specimens suitable for collection of x-ray diffraction data (Caspar et al., 1977; Makowski et al., 1984*a*).

Diffraction patterns were recorded on film from specimens mounted in quartz capillaries using x-rays of wavelength $\lambda = 1.54$ Å produced by a rotating-anode generator and focused by a double-mirror or germanium monochromator camera. The optical densities of the films were digitized on a rotating drum densitometer (Optronics International, Chelmsford, MA) interfaced to a node in the Rosenstiel VAXCluster (Digital Equipment Corp., Maynard, MA). The value of the optical density near the unexposed edge of the film arising from chemical fog was subtracted from the entire pattern, and intensities were symmetry averaged about the best equatorial and meridional axes. Due to curvature of the sphere of reflection, the geometrically corrected pattern (Fraser et al., 1976) shows a region of reciprocal space near the meridian not recorded on the film (Fig. 1). The Bragg spacing of a diffraction maximum in angstroms is the reciprocal of its radial coordinate $D = 2 \sin\theta/\lambda$ measured in angstroms^{-1}. The components of the diffraction vector **D** in cylindrical coordinates are **Z** normal to the mean orientation of the membrane plane, and **R** perpendicular to this axis.

The data were separated into two parts: a broad, nearly circularly symmetric band of diffuse scatter that rises smoothly from ~0.15 Å^{-1} and a component of diffracted intensity showing a characteristic modulation reciprocally related to the connexon pair dimensions. This modulated component was smoothed over a small range of orientations by convolution with a Gaussian of standard deviation 5°. The spherically averaged distribution of intensity (Fig. 2) was calculated by multiplying each intensity element in the modulated component by its distance from the meridian, then averaging over all angles to the meridian.

Fourier transformation of protein structures

The modulated high-angle diffraction from gap junctions is due to ordered domains of protein embedded within the membranes in less

regular matter of comparable electron density. We have developed a procedure to calculate the scattered intensity due to the internal structure of a protein molecule, separated from the shape contribution, to compare with these patterns.

Electron density maps of proteins in vacuum were constructed using coordinates from the Brookhaven Protein Data Bank (Bernstein et al., 1977) and other sources (see Fig. 3) by placing a Gaussian sphere $\rho_A(r)$ at the position of each nonhydrogen atom to represent n_A scattering electrons:

$$\rho_A(r) = n_A\Omega(r; \sigma_A). \quad (1)$$

The standard deviation of the Gaussian $\Omega(r; \sigma_A)$ was

$$\sigma_A = (\delta^2 + \epsilon^2)^{1/2}, \quad (2)$$

where δ was the root mean square displacement of the atom due to thermal disorder and ϵ was the standard deviation of the electron density distribution of the atom. The value of δ^2 was obtained from the crystallographic temperature factor $B = 8\pi^2\delta^2$ and ϵ was evaluated from the Fourier transform of a Gaussian approximation to the carbon atomic form factor. The mean value of δ for well-ordered crystalline proteins is ~0.5 Å and ϵ = 0.35 Å for carbon, thus $\sigma_A \approx 0.6$ Å for the nonhydrogen atoms. The contribution of the hydrogen atoms bound to the atom A were represented by a Gaussian sphere $\rho_H(r) = n_H\Omega(r; \sigma_H)$, superimposed on $\rho_A(r)$, with standard deviation $\sigma_H > \sigma_A$. The value of σ_H was set equal to the radius of the sphere which approximates the expected volume of the atom A and its bound protons (Richards, 1974).

The protein surface was defined as the density contour in the three-dimensional map of the protein in vacuum which enclosed a volume equal to the sum of the expected amino acid residue volumes (Richards, 1974; Chothia, 1975). The protein shape map was constructed by averaging the protein density over its interior and setting exterior volume elements to zero. To soften the edge of this "hard" shape, its Fourier transform was multiplied by a Gaussian of standard deviation 0.2 $Å^{-1}$ and back-transformed. The softened shape map was then subtracted from the map of the protein in vacuum, and the transform of this difference calculated. The squared transform of the protein-shape difference map thus represented the expected diffraction due to ordered domains of protein embedded in a medium of matching electron density.

Disorientation and cylindrical averaging

Comparison of calculated intensity distributions with the gap junction diffraction data depends critically upon introduction of disorientation and rotational disorder into the calculated patterns. Imperfect parallel orientation of the membrane planes smears a diffraction vector **D** into a disk, with radius of curvature D, according to the disorientation distribution. Random rotation of the lattice plane about the membrane normal spreads this disk of intensity into an annulus, with radius of curvature D, centered about the orientation axis. The angular distribution of intensity in the annulus depends on the disorientation distribution and the angle of the unsmeared spot to the meridian, but is independent of D. A distribution lookup table, calculated at 1-degree intervals over the range of angles to the meridian, was used to rapidly smear the model pattern in spherical polar coordinates. The smeared pattern, in cylindrical coordinates, corresponds to the central section of the cylindrically symmetric pattern derived from the digitally processed diffraction photographs.

Model building

Connexonlike hexamers were constructed from two different four α-helix bundle proteins and a three-stranded coiled coil (Fig. 5, *a–c*) using FRODO (Jones, 1978). For the models built from ferricytochrome *c'* and TMV protein, the molecules were rotated about the *z*-axis and translated radially, starting from the tilted orientations shown in Fig. 4, *c* and *d*, in an interactive search for plausible packing arrangements of the six symmetry-related helix bundles. The hexamer of three α-helix segments was constructed from the coiled-coil portion of the influenza virus hemagglutinin trimer with its threefold axis tilted ~10° to the hexamer axis. Dodecamers were created by placing twofold axes perpendicular to the sixfold such that the centers of mass of the helices would lie ~85 Å apart. The length, pitch, location, and tilt of helical segments in the dodecamer models are listed in Table 1.

RESULTS

The diffraction data from the gap junction specimens were separated into two parts: one part due to the protein structure that is coherently ordered within the pair of connexon hexamers; and the other from the water, lipid, and disordered portions of the protein that have coherence distances much smaller than the 60 Å diameter of the connexon. Diffraction from the ordered part shows a characteristic modulation that is reciprocally related to the connexon pair dimensions, whereas the diffuse scatter from the disordered components is nearly circularly symmetric and rises smoothly to a broad maximum at ~3 Å spacing. Separation of these components (Fig. 1) was facilitated by comparison of diffraction patterns from three specimens, containing different proportions of water and lipid, which show very similar modulated protein diffraction with different diffuse backgrounds.

Spherically averaged patterns

The spherically averaged intensity distribution indicates the type of secondary structure present, independent of its orientation. Different crystalline proteins within a given tertiary structure class (Richardson, 1981) show similar spherically averaged intensity distributions (Fig. 2, *a-c*), regardless of the amino acid sequences and variations on the common scheme of chain folding. All show comparable maxima between 4 and 5 Å spacing, whereas the relative strength of the 11 Å spacing peak is correlated with the α-helix content (Fig. 3). The ratios of mean intensity in the 11 Å peak compared with that at 5 Å spacing range from 2.0 for a coiled-coil to ~0.75 for a β-barrel. Comparison of the spherically averaged gap junction diffraction data with intensity distributions calculated for different proteins indicates that the ordered portion of the connexon is at least 60% α-helical (Fig. 3), and among the proteins compared, the four α-helix bun-

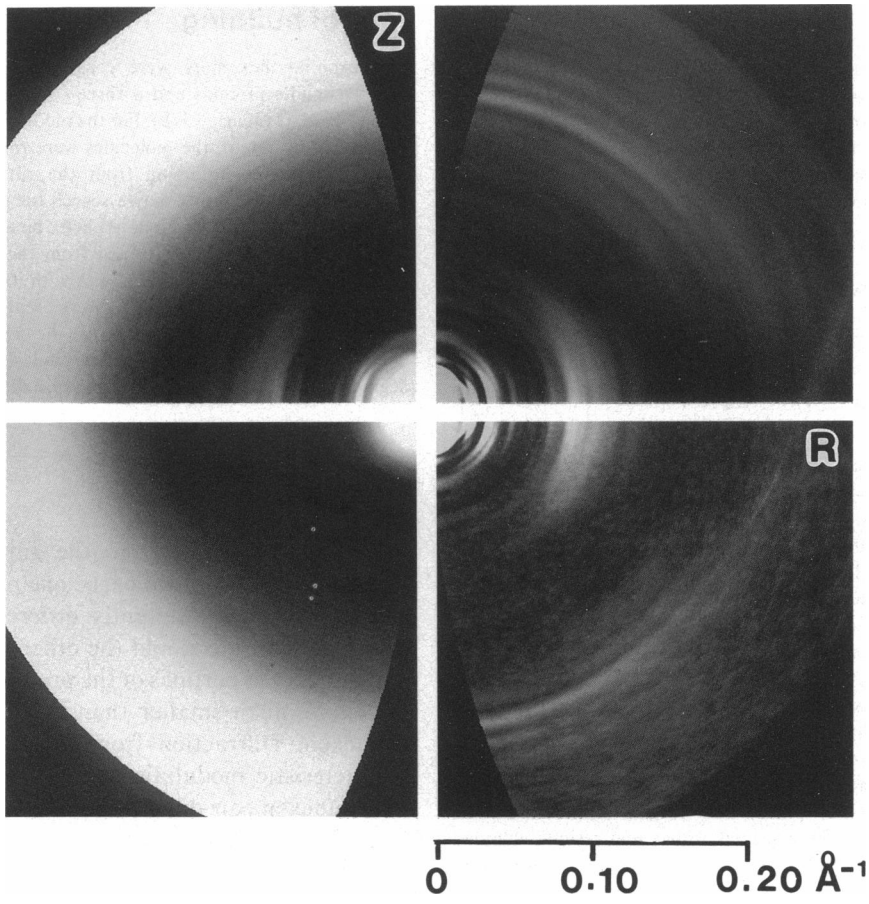

FIGURE 1 Diffraction data from oriented gap junction membranes. The pattern obtained from mouse liver specimen L68 is shown in the upper left corner after quadrant averaging, subtraction of film fog, and conversion to cylindrical polar coordinates (R, Z) in reciprocal space. Intensity near the meridian is missing due to the curvature of the sphere of reflection. These data were resolved into two components: modulated intensity arising from coherently ordered protein within the connexon (*lower right*) and diffuse scatter from disordered protein, lipid, and water (*lower left*). The modulated component was angularly smoothed by convolution with a Gaussian of 5° standard deviation to further reduce noise (*upper right*).

dle structures have diffraction profiles which correspond most closely with the gap junction data (Fig. 2 *a*).

Cylindrically averaged patterns

Cylindrically averaged diffraction patterns of imperfectly aligned α- and β-proteins were calculated from their Fourier transforms to assess how the orientation of structural domains could be inferred from the gap junction diffraction data. The backbones of two β-and two α-proteins are shown at the left of Fig. 4, oriented to give a meridional diffraction maxima at ~4.8–4.9 Å spacing; and their calculated diffraction patterns are shown at the right in Fig. 4, after convolution with a ±15° disorientation distribution and cylindrical averaging.

The sharpness of the meridional maxima is related to the axial extent of the periodic secondary structure. To produce a maximum on the meridian beyond 0.2 Å^{-1} for ferricytochrome c' and TMV proteins, the orientation angles of some of the α-helices in each molecule were set at angles >20° to the reference z-axis, with a standard deviation of ~±13° for the range of tilts of the individual segments. If all four α-helices were aligned nearly parallel to the axis, then the maximum of the ~5.4 Å pitch spacing layer line would have occurred off the meridian.

The distinguishing feature of the cylindrically averaged α-helical diffraction, in contrast to the β-sheet patterns, is the dominant equatorial maximum at 11–12 Å spacing. The angular width of this maximum is determined by the orientations of the α-helical segments relative to the reference axis, the orientation distribution, and the intrinsic off-equatorial width of the diffraction (which is related to the axial length of the segments). The ~25° angular half-width of the 11–12 Å spacing arc in the computed disoriented patterns is comparable with that measured in the gap junction patterns. Thus, a bundle of

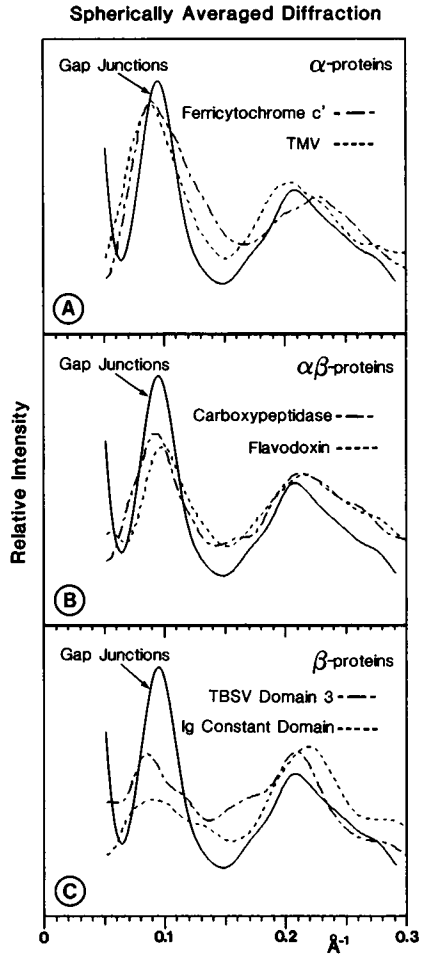

FIGURE 2 Spherically averaged intensity distributions calculated from Fourier transforms of proteins representing different structural classes. Gap junction spherically averaged diffraction, shown in each frame, was generated from the cylindrically symmetric modulated intensity (Fig. 1) by weighting each grid point by its distance R from the meridian, then integrating over all angles to the meridian. The resulting curve was low-pass Fourier filtered (with a 17-Å resolution cutoff) and scaled with the calculated curves to have the same integrated intensity in the 4–5 Å spacing peak. The gap junction maxima near 10 Å falls close to curves calculated for two four-helix bundle proteins, *Rhodospirillium* ferricytochrome c' and tobacco mosaic virus (TMV) coat protein (*A*). Flavodoxin, a parallel β-sheet structure surrounded by α-helices, and carboxypeptidase, a mixed-sheet structure surrounded by α-helices, give maxima near 10 Å smaller than that in the gap junction data (*B*). Antiparallel β-sheet structures have even smaller maxima near 10 Å, as shown by curves calculated for tomato bushy stunt virus (TBSV) domain 3, an eight-stranded β-barrel, and the Bence Jones protein, an immunoglobin constant domain β-barrel (*C*).

α-helices set at a mean orientation angle ψ of ~20° to the membrane normal, with a variation of 10–15° in the tilt angles and a disorientation distribution of ±15°, is consistent with the angular width of the equatorial arcs in the diffraction pattern recorded from the coherently ordered protein in the gap junction connexons.

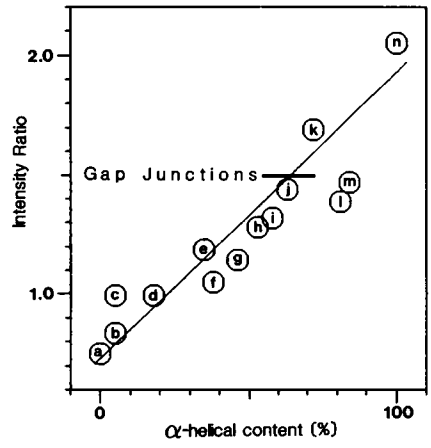

FIGURE 3 Relation of the peak intensity ratio in spherically averaged diffraction patterns to the α-helical content of the protein. The ratio of average intensity in the interval 0.07–0.11 $Å^{-1}$ to that in the interval 0.18–0.23 $Å^{-1}$ is correlated with helix content of the ordered portion of the structure (those residues having an average Debye factor of <60 $Å^2$). (*a*) Immunoglobin light chain constant domain, a simple antiparallel β-barrel (Xu and Schiffer, 1988) (*b*). Plastocyanin, also a simple antiparallel β-barrel (Guss et al., 1986). (*c*) Domain 3 of TBSV coat protein, an antiparallel jellyroll β-barrel (Hopper et al., 1984). (*d*) Subtilisin inhibitor, an antiparallel β-sheet with transverse α-helix (Mitsui et al., 1979). (*e*) Carboxypeptidase, an $\alpha\beta$ mixed-sheet structure (Rees et al., 1983). (*f*) Flavodoxin, a parallel β-sheet surrounded by α-helices (Smith et al., 1977). (*g*) Lactate dehydrogenase, structurally similar to flavodoxin (Musick and Rossman, 1979). (*h*) Insulin subunit, a small $\alpha\beta$ protein in the cubic crystal form (Badger et al., manuscript in preparation). (*i*) Triose phosphate isomerase, a parallel β-barrel surrounded by α-helices (Banner et al., 1976). (*j*) TMV coat protein, an antiparallel up-down helix bundle (Namba and Stubbs, 1986). (*k*) Ferricytochrome c', an up-down divergent bundle of four antiparallel α-helices (Finzel et al., 1985). (*l*) Hemoglobin β-subunit, an antiparallel helix bundle (Bolton and Perutz, 1970). (*m*) *E. coli* repressor of primer (ROP), an antiparallel up-down four-helix bundle with twofold symmetry (Banner et al., 1987). (*n*) Three strands of residues 96–115 from influenza virus hemagglutinin, related by a threefold axis in a parallel-stranded coiled coil (Wilson et al., 1981).

Diffraction from the connexon pair and dodecamer models

To simulate the high spatial frequency modulation of the gap junction data, we have calculated cylindrically averaged, disoriented diffraction patterns of dodecamers with 622 point group symmetry, built from three- and four-stranded α-helix proteins arranged to give dimensions similar to the channel-forming pair of connexon hexamers (Fig. 5). The models were built with the centers of the α-helical domains 42–44 Å above the midplane, corresponding to the 42 Å distance of the gap junction bilayer center from the middle of the gap (Makowski et al., 1977, 1984*b*); and the mean radii of the α-helix bundles were set

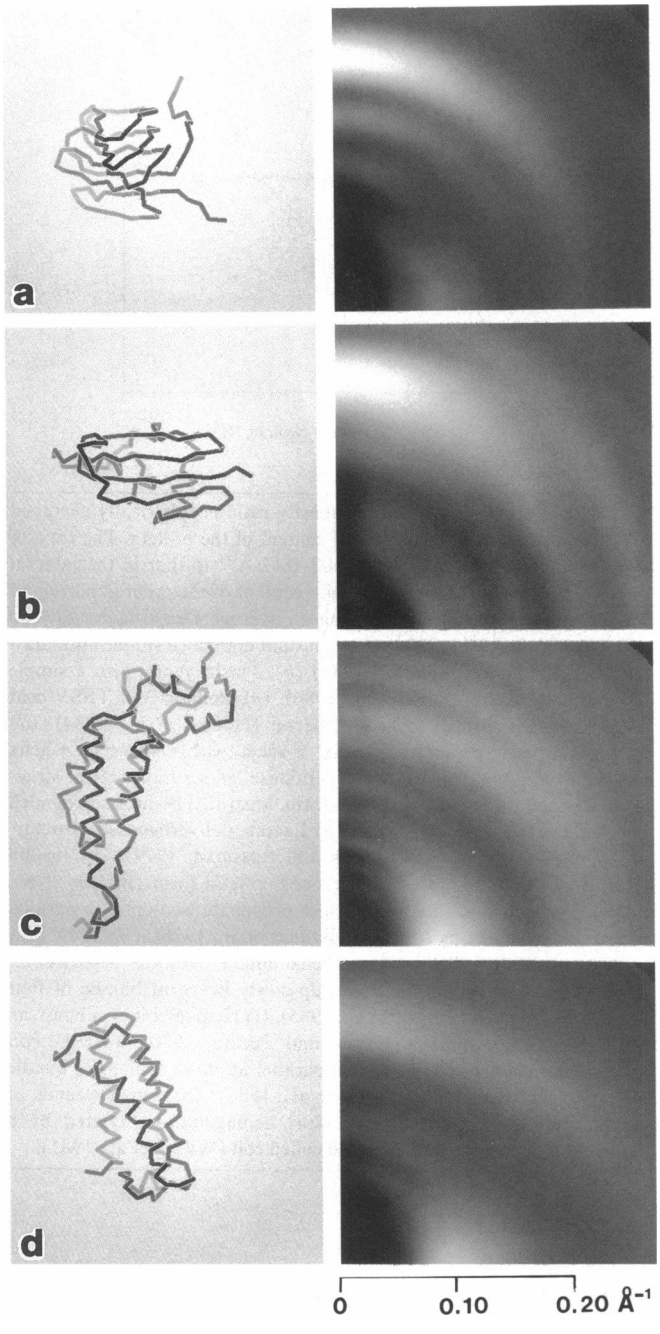

FIGURE 4 Comparison of cylindrically averaged, disoriented intensity distributions calculated from Fourier transforms of up-down α-helical bundles and cross β-sheet models. Domain 3 of TBSV protein (*a*) and *Streptomyces* subtilisin inhibitor (*b*) were oriented with their antiparallel β-strands running nearly perpendicular to axis of orientation. TMV coat protein (*c*) and ferricytochrome *c'* (*d*), each containing a bundle of four α-helices, were positioned such that mean tilts of the segments to the vertical orientation axis were, respectively, 18 and 23°. Diffraction patterns calculated from transforms of these proteins, after convolution with the ±15° disorientation distribution, circular averaging, and scaling to the same peak intensity are shown on the right. The α-helical bundles give rise to intensity distributions that correspond to the distribution of the modulated intensity in the gap junction diffraction pattern: an equatorial diffraction maxima near 0.09 Å^{-1} and a meridional maxima, of approximately equal magnitude, near 0.21 Å^{-1}. Diffraction patterns from the cross-β models show a stronger meridional peak, relative to the equatorial maximum, than is observed in the gap junction data.

at 22–25 Å from the hexamer axis as expected for the channel-forming portion of the connexon with a minimum inner radius of ~10 Å and a maximum outer radius of 35 Å (Unwin and Ennis, 1984; Makowski et al., 1984*b*). The length (L) and pitch (p) of the individual α-helix segments (Table 1) are defined by the atomic coordinates of the influenza hemagglutinin coiled-coil domain (Wilson et al., 1981), the TMV protein subunit (Namba and Stubbs, 1986) and ferricytochrome *c'* (Finzel et al., 1985) which were used to build the dodecamer models. The α-helical segments in these proteins are about long enough to span a lipid bilayer and wide enough to form a compact hexamer with the diameter of the connexon.

Within the restraints of constructing model dodecamers from the three selected α-helical proteins arranged to resemble a pair of connexon transmembrane channels, as much variation as seemed plausible was introduced in the tilts and coordinates of the individual segments among the three models (Table 1). The objective of this model-building exercise was to correlate features in the calculated diffraction patterns with the model parameters as a guide to determining the number, mean length, radius, height and tilt of the α-helical segments in the connexon pair.

Meridional diffraction in the 5 Å spacing region of the gap junction and model dodecamer diffraction patterns (Fig. 5) arises from the ~5.1 Å distance between successive turns of polypeptide chain coiled in the α-helices of pitch ~5.4 Å. The sharp fringes are a modulation of the α-helix pattern determined by the ~80 Å distance between the symmetrically related pairs of domains. The overall meridional extent of the strong set of fringes is inversely proportional to the length of the helix segments. The position of maximum intensity among these fringes depends on the tilt of the α-helix segments relative to the hexamer axis as well as on the pitch spacing.

Equatorial diffraction in the 11 Å spacing region (Fig. 5) arises from the scattering contrast between the dense backbones and low-density side chains of the α-helices that are nearly aligned and compactly packed. The high spatial frequency modulation along the equator is dependent on the number and cylindrical coordinates of the α-helical segments in the monomer unit forming the hexamer. The angular distribution of intensity in the equatorial arc depends on the tilts of the α-helix segments relative to the hexamer axis and on the disorientation distribution.

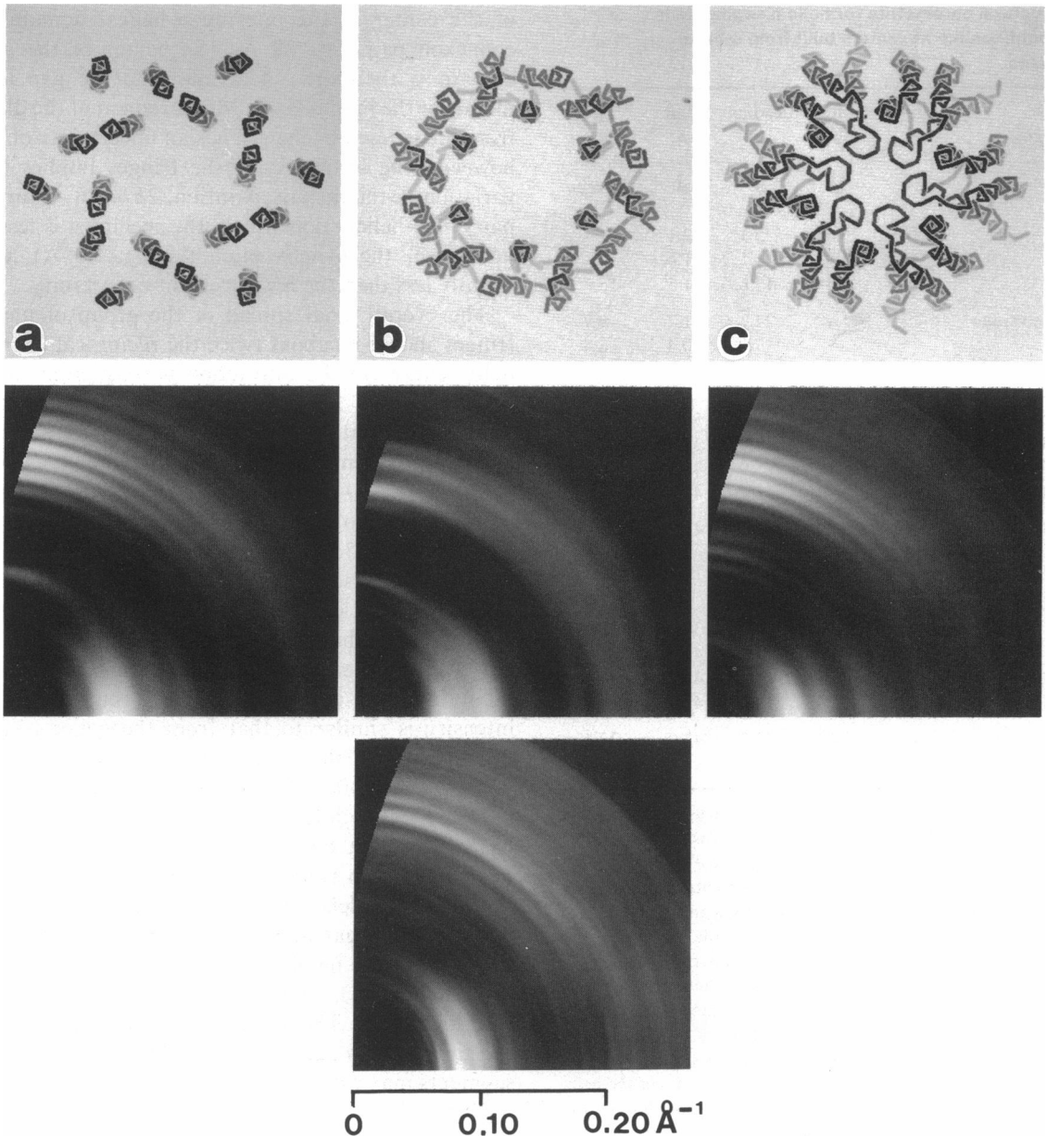

FIGURE 5 Connexonlike models of α-helical bundle proteins and comparison of their diffraction patterns to data from ordered protein in gap junction membranes. The model hexamers in the upper row are viewed along the sixfold axis, and the corresponding diffraction patterns from pairs of these hexamers with the mean orientation of their axes vertical are shown below them in the middle row. The model at the left (*a*) was constructed from three-stranded coiled coils oriented ~10° to the hexamer axis. In the center (*b*) and at the right (*c*) are models made from four-stranded helix bundle proteins with the orientations shown in Fig. 4, *c* and *d*. The size, location and tilt of helices in the connexon were estimated by comparing the angular distribution in the equatorial arc at 0.09 Å^{-1} and the frequency of modulation in the meridional intensity near 0.21 Å^{-1} in the model patterns to that observed in the data (*bottom row*).

Meridional data

The periodicity of the sharp meridional fringes, as a function of the Z reciprocal space coordinate, is defined by the wavelength of the functions $\exp(-2\pi iZh_j)$ that modulate the transform of the jth pair of α-helices whose centers are located at a height h_j from the midplane. Modulations of the intensities of these fringes depend on the phase relations of the transforms of the different pairs of segments, which are determined by the detailed structure and packing arrangement of the α-helices; but the mean wavelength of the modulation (i.e., twice the fringe

TABLE 1 Structural parameters for helical segments in dimers of connexonlike hexamers built from α-helix bundle proteins

Helix segment	Length L	Pitch p	Radius r	Height h	Tilt ψ
	Å	*Å*	*Å*	*Å*	*degrees*
HA_2					
F 96–115	29.9	5.48	25.1	42.1	11
B 96–115	29.9	5.48	31.5	41.4	2
C 96–115	29.9	5.48	17.6	41.5	15
Weighted average	29.9	5.48	24.7	41.7	9.7
±SD	—	—	±7.0	±0.4	±6.5
TMV					
LS 19–32	19.5	5.34	23.0	50.7	33
RS 38–48	15.0	5.31	28.8	39.0	23
RR 73–87	22.2	5.80	25.9	45.6	26
LR 111–135	36.3	5.48	17.2	41.9	2
Weighted average	25.8	5.49	22.4	44.2	17.8
±SD	±8.6	±0.18	±4.5	±4.0	±12.9
Ferricytochrome *c'*					
A 5–30	37.3	5.80	23.1	38.0	38
B 40–53	19.9	5.39	27.8	46.1	31
C 79–102	34.8	5.32	27.1	43.3	16
D 104–125	32.3	5.54	18.2	42.7	6
Weighted average	32.5	5.53	23.7	42.0	22.5
±SD	±5.9	±0.19	±3.7	±2.9	±12.9

Helix designations are those assigned for influenza virus hemagglutinin (HA_2) by Wilson et al., (1981), for tobacco mosaic virus protein (TMV) by Champness et al., (1976), and for ferricytochrome *c'* by Finzel et al. (1985). The length L and pitch p of the helix segments are defined by atomic coordinates. The rise per residue in the helix segments is equal to the length divided by the number of peptide bonds; the average for the eight segments is 1.53 ± 0.04 Å. The average number of residues per turn in these helices is 3.62 ± 0.13, from the ratio of the pitch to the rise per residue. The radius r, height h, and tilt ψ of the α-helical segments in the models have been set by rigid body adjustments of the positions of the protein molecules to form hexamers with diameters similar to that of the connexon. The r and h coordinates of the center of mass of the helix segments are measured from the sixfold axis and the midplane of the 622-point group, respectively. The tilt angles ψ of the helix axes are measured relative to the sixfold axis direction. Parameter values were weighted in mean values by the number of residues for that segment. SD is the square root of the mean weighted square residuals.

width) is close to $1/\bar{h}$, the reciprocal of the distance from the midplane to the center of the α-helical domain. For example, in the two models in Fig. 5 built with $\bar{h} \approx 42$ Å (Table 1) the fringe wavelength is ~0.023 $Å^{-1}$; for the TMV protein model with $\bar{h} = 44$ Å, the wavelength of the modulation is nearly the same, but the central fringe is extinguished due to interference.

In the gap junction pattern, the wavelength measured for the four distinct fringes centered at $Z \approx 0.205$ $Å^{-1}$ is ~0.026 $Å^{-1}$; thus, the mean height $\bar{h}$ above the midplane of the center of the inferred α-helical domains in the connexon pairs is ~38 Å. The center of the α-helical domain is therefore ~4 Å closer to the gap than the middle of the lipid bilayer. Measurement of the distance $\bar{h}$ from the fringe wavelength has an uncertainty of ±2–3%; however, the sharpness of the fringes implies that the variation in the mean separation, $2\bar{h} \approx 76$ Å, among the pairs of α-helical domains in the specimen is less than a quarter of the α-helix pitch (i.e., $< \pm 1.3$ Å), which is slightly less than the measurement uncertainty.

The overall axial spread of the group of meridional fringes should be about twice the reciprocal of the mean helix length. In the diffraction pattern from the model built with the hemagglutinin three-stranded coil–coil domain of length $L = 29.9$ Å (Fig. 5 *a*, Table 1), the envelope of intensity of the fringes can be fit, as expected, to $\sin[\pi(D - D_0)L]/\pi(D - D_0)L$ with $D_0 = 0.195$ $Å^{-1}$, corresponding to the position of maximum intensity determined by the ~5.1 Å spacing of the α-helix turns. Helices in the model based on ferricytochrome *c'* (Fig. 5 *c*, Table 1) have a mean length of $\bar{L} = 32.5$ Å, with a larger range of tilts than the coiled-coil model; in the calculated diffraction pattern of this model, the position of maximum intensity is $D_0 \approx 0.21$ $Å^{-1}$, but the spread of intensity is similar to that from the coiled-coil model, consistent with the similar mean helix lengths. In the TMV-based model (Fig. 5 *b*) the LR helix of length 36.3 Å, which is much longer than the other three (Table 1), has a dominant effect on the spread of the meridional intensity, which is slightly narrower than that from the other two models (Fig. 5). The spread of meridional intensity in the gap junction pattern is ~10–20% narrower than that in the model coiled-coil and ferricytochrome *c'* patterns (Fig. 5), which indicates that the mean α-helix length is >30 Å. The distribution of the fringe intensity in the gap junction pattern suggests that the longest α-helix segments may extend ~40 Å.

The position of maximum intensity on the meridian in the patterns from disoriented α-helices will occur near $Z = 0.196$ $Å^{-1}$, which is the reciprocal of the 5.1 Å chain spacing, if the tilt, ψ, of the helix segments relative to the hexamer axis is less than the 19° α-helix pitch angle. This is the case for the coiled-coil model for which $\bar{\psi} = 9.7°$. For tilt angles, $20° < \bar{\psi} < 40°$, the position of the maximum should shift out to $Z \approx (p \cos\psi)^{-1}$. In the ferricytochrome *c'* model pattern (Fig. 5 *c*), the maximum intensity at $Z \approx 0.21$ $Å^{-1}$ corresponds to $\psi \approx 28°$; because the mean tilt of the model is 22.5° (Table 1), it appears that the more tilted segments have a dominant effect on the meridional intensity distribution. The maximum in the intensity envelope of the gap junction meridional fringes at $Z \approx 0.205$ $Å^{-1}$ thus indicates a weighted tilt of ~25° for helices of pitch 5.4 Å.

Equatorial data

The equatorial intensity distribution is related by the cylindrical Bessell function terms $[J_n(2\pi Rr_i)$ of order $n = 0, 6, 12 \ldots]$ to the radial coordinates r_i, measured from the hexamer axis, of the helix segments. Because the side-to-side spacing of the α-helix segments is ~10–13 Å, the maximum intensity will occur near $R \approx 0.09$ Å^{-1}, with a spatial frequency modulation characteristic of the radial coordinates. The widths of equatorial maxima in the diffraction patterns of the ferricytochrome c' and hemagglutinin coiled-coil models (Fig. 5) are similar because the mean radii of the α-helical segments are $\bar{r} \approx$ 24 Å in both models, even though one model has four segments and the other three. These two patterns differ in the position of the maximum because the distance between α-helix segments is larger in the influenza coiled-coil than in ferricytochrome c'. The position of the maximum in the TMV-based model is near 0.09 Å^{-1} and the arc width is similar to that of the other two model patterns (Fig. 5), although there are differences in the details of the intensity modulation due to detailed differences in the structures.

The gap junction pattern was Fourier filtered to remove the sharp lattice sampling from the data for comparison with the model diffraction patterns (Fig. 5). The correspondence in the overall width of the 0.09 Å^{-1} maximum in the gap junction pattern with that of the model equatorial diffraction maxima indicates that there are three or four near axial α-helix segments in the connexon subunit which are located at a mean radius $\bar{r} \approx$ 24 Å in the hexamer. To compare the profile of the 0.09 Å^{-1} maximum from the gap junctions and the ferricytochrome c'–based model, the patterns were smoothed with the same low-pass Fourier filter, spherically averaged and scaled in the interval 0.18–0.23 Å^{-1} (Fig. 6 *a*). The similarity in width of the maximum characteristic of the 24 Å mean radius is evident from this comparison. However, the slightly lower integrated intensity of the 0.09 Å^{-1} peak for the gap junction pattern compared to that for the model ferricytochrome c' pattern indicates that the α-helix contents are in proportion to this intensity ratio (*cf.* Fig. 3).

The equatorial arcs in the model disoriented patterns (Fig. 5) have angular half-widths of about $(\phi^2 + \bar{\psi}^2)^{1/2}$, where ϕ is the half-width of the disorientation distribution and $\bar{\psi}$ is the mean orientation angle of the α-helices relative to the hexamer axis (Table 1). In the three-stranded coil–coil model pattern (Fig. 5 *a*), the angular half-width of the equatorial arc is ≈19° corresponding to the 10° average helix tilt convoluted with the ±15° disorientation distribution. Similarly, the arc widths for the TMV protein and ferricytochrome c' patterns are 23°

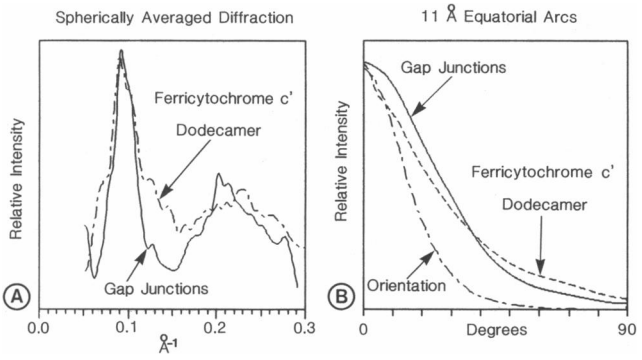

FIGURE 6 Spherically averaged diffraction (*A*) and the angular distribution of equatorial intensity (*B*) in the cylindrically averaged pattern from a pair of ferricytochrome c' hexamers compared to curves from the gap junction data. A 100 Å resolution low-pass Fourier filter was applied to the spherically averaged ferricytochrome c' dodecamer intensity distribution and to the spherically averaged diffraction data; this removed the effects of hexagonal lattice sampling in the data. The angular spread of the gap junction disorientation distribution (shown in *B* as measured from the small-angle meridional fringes) depends only upon the orientation of the membranes, and is not as broad as ~11 Å spacing equatorial arcs in the data. The angular spread of the equatorial arcs in the model, which is similar to that of the gap junction data, is due to the 23° mean tilt of the α-helices combined with the 15° standard deviation of the orientation distribution.

and 27° corresponding respectively to mean α-helix tilts of 18° and 23°. The angular distribution of the equatorial maximum in the gap junction pattern is compared with that of the ferricytochrome c' model in Fig. 6 *b*. Because the half-widths of these two patterns are similar, it appears that the α-helices in the connexon, like those in the model, are oriented at a mean angle of ~20° to the hexamer axis. The spread of orientations in the connexon appears to be narrower than in the ferricytochrome c' model, since the measured intensity distribution for the equatorial arc from the gap junctions lies above that for the simulated patterns at angles smaller than the half-width and below at larger angles; from this comparison of the shapes of the curves, the standard deviation for the tilt angles in the connexon is estimated to be ~10°.

Summary of α-helical parameters

About 60% of the ordered portion of the connexon is α-helical, as indicated by the ratio of intensity in the 0.09 and 0.20 Å^{-1} spacing peaks in the spherically averaged diffraction data. In the cylindrically averaged pattern, the overall spread of the meridional fringes in the axial direction between $Z = 0.18$ and 0.24 Å^{-1} indicates that the mean length of $\bar{L}$ of the helix segments is ~35 Å and the maximum helix segment length is ~40 Å. From the average width of the meridional fringes, the mean dis-

tance $\bar{h}$ from the midplane of the gap junction to the centers of the α-helix segments, is 38 ± 1 Å. The angular distribution of intensity in the 0.09 $Å^{-1}$ equatorial arc indicates that the mean segment tilt is $\bar{\psi}$ is ~20°, in agreement with the estimate from the position of the maximum meridional intensity, and the variation in orientation of the segments relative to the mean is ~10°. From the radial modulation of the 0.09 $Å^{-1}$ equatorial arc, there appear to be three or four near axial helix segments per subunit located at a mean radius of 24 ± 2 Å in the hexamer.

DISCUSSION

Maps of connexin chain topologies in gap junctions, deduced from binding of antibodies and susceptibility to proteolysis (Hertzberg et al., 1988; Milks et al., 1988; Goodenough et al., 1988), show four transmembrane segments, identified with the four hydrophobic sequences in the molecules (Paul, 1986; Kumar and Gilula, 1986; Beyer et al, 1987; Gimlich et al., 1988). By analogy with other membrane proteins, the hydrophobic transmembrane segments have been presumed to be α-helical (Unwin, 1986; Hertzberg et al., 1988; Milks et al., 1988). Our analysis of the x-ray diffraction data from oriented gap junction specimens shows that the transbilayer portion of the connexin molecule is largely α-helical. Comparison with diffraction patterns calculated for models constructed from α-helical proteins provides a measure of the overall α-helix content in the ordered portion of the connexon, the number of transmembrane helices per monomer and their mean length, position, and orientation in the hexamer.

Are all four transmembrane segments completely α-helical? The modulation of the 11 Å spacing equatorial diffraction maximum is compatible with three or four α-helix segments at a mean radius of 24 ± 2 Å. The strength of the higher spatial frequency modulation indicates that, at least, the three transmembrane segments forming the surface of the hexamer in contact with lipid hydrocarbon are helical, in accord with physicochemical expectation. The four hydrophobic connexin sequences consist of from 20 to 30 residues and constitute about half the portion of the molecule mapped within the membrane bilayer and gap (Hertzberg et al., 1988; Milks et al., 1988; Goodenough et al., 1988). Assuming that only the cytoplasmic portion of the connexon is disordered, the α-helix content of ~60% in the ordered portion, estimated from the x-ray intensity measurements, suggests that some part of the protein in the gap, as well as the transbilayer segments, may be α-helical.

The lengths of the four hydrophobic segments should range from ~30 to 45 Å, if completely α-helical. Because the hydrocarbon core of the bilayer is ~32 Å thick (Makowski et al., 1977, 1984*b*), the shortest helical segment could just span this distance, and the longest segment, if completely immersed within the bilayer, could be inclined by ~45° to the connexon axis. The mean axial projected length of at least 30 Å and mean tilt of ~20° for the helical segments deduced from the x-ray data are therefore consistent with the measured bilayer thickness and the inferred lengths of the hydrophobic sequences. If the transmembrane helices were confined to the hydrocarbon layer, their centers should all be located at the middle of the bilayer, which is ~42 Å from the midplane of the gap (Makowski et al., 1977). Because the length of some helix segments appear to exceed the bilayer thickness, and the center mass of the α-helical domain is ~4 Å closer to the gap than the bilayer center, it is likely that some helical structure extends into the level of the polar layer on the gap side. Thus, the x-ray diffraction data indicate that most of the four transmembrane segments are α-helical and that some α-helical structure extends into the gap portion of the connexon.

What part of the connexin molecule is disordered? The cytoplasmic portion of the connexon structure, extending from the bilayer surface at ~70 Å from the gap center out to ~90 Å, as seen in the membrane profile calculated from ~25 Å resolution x-ray diffraction data (Makowski et al., 1984*b*) and under some conditions by electron microscopy (Caspar et al., 1988; Sosinsky et al., 1988) appears to be quite flexible. This part of the structure can disorder sufficiently to become invisible in the averaged three-dimensional reconstructions from micrographs of negatively stained (Unwin and Zampighi, 1980) and frozen-hydrated specimens (Unwin and Ennis, 1984). Flexible portions that have coherence lengths much smaller than the connexon diameter do not contribute to the modulated high-angle diffraction due to the rigidly packed transmembrane α-helices and ordered portions in the gap. The cytoplasmic parts, which have the most variable sequences among different connexins (Beyer et al., 1987; Gimlich et al., 1988), may have some locally ordered secondary structure but, without longer range ordering, it would be difficult to characterize such structure from the diffraction data.

How invariant is the protein structure within the bilayer and gap? The sharpness of the meridional diffraction fringes in the 5 Å spacing region shows that the transmembrane α-helical domains, linked together at the gap within each connexon pair, are as rigid as protein molecules in well-ordered crystals. Some portions of the connexon near the cytoplasmic membrane surface and facing the transmembrane channel may be more mobile, in particular, the part forming the gating structure identified at the mouth of the channel (Makowski, 1985). The invariance of the meridional diffraction fringes observed

in the ~4 Å resolution x-ray diffraction data when the lipid and water content, and the calcium concentration are varied (Caspar et al., 1988), and when the labile cytoplasmic portions of the protein are proteolyzed (Makowski et al., 1984*b*) indicates that the transmembrane α-helical domains remains fixed within the connexon pairs under conditions that alter their packing arrangement or affect the gating. Thus it appears unlikely that gating involves twisting and tilting of the transmembrane part of the connexin molecules as previously inferred from ~25 Å electron microscopy data (Unwin and Zamphigi, 1980; Unwin and Ennis, 1984). Considering the close homologies of the sequences mapped within the bilayer and gap for different connexins (Beyer et al., 1987; Gimlich et al., 1988), it is likely that this portion of these molecules forms similar rigid channel structures in all gap junction membranes.

Can the molecular structure of the ordered part of the connexon channel be determined from the diffraction data from noncrystalline oriented specimens? This problem is analogous to the determination of the atomic resolution structure of tobacco mosaic virus from oriented fiber patterns (Namba and Stubbs, 1986); thus, given sufficient restraining information to separate and phase overlapping lattice reflections in the cylindrically averaged, disoriented pattern, the structure could be solved to high resolution. A 16 Å resolution map has been calculated using an iterative model-refinement procedure (Tibbitts et al., 1988) starting with the lower resolution three-dimensional reconstruction from electron micrographs of frozen-hydrated specimens (Unwin and Ennis, 1984). Extension of this refinement beyond 10 Å resolution to visualize the packing of the transmembrane α-helices, whose mean size, location, and orientation have been estimated in this study, will require additional structural information from higher-resolution electron micrographs of unstained specimens and/or isomorphous derivative x-ray diffraction data from better ordered gap junction preparations.

This work was suported by United States Public Service grants CA47439 from the National Cancer Institute to D. L. D. Caspar and GM18940 from NIGMS awarded to D. A. Goodenough.

Received for publication 17 May 1989 and in final form 27 December 1989.

Note added in proof: Our diffraction diagnosis has indicated that there is more near-axial α-helix in the connexon than can be accounted for by just the transmembrane segments. Diffraction patterns have therefore been calculated from model structures for the connexon pair which include α-helical segments in the gap portion of the structure. Interference between scattering from similarly oriented α-helical domains in the bilayer and gap can broaden the apparent angular width of the 0.09 $Å^{-1}$ equatorial arc and alter the intensity distribution in the meridional fringes. For example, a model with three α-helical segments in the gap and in the bilayer oriented nearly parallel to the connexon axis can account for the observed intensity distribution in the 0.09 $Å^{-1}$ equatorial arc. Thus, the mean orientation of the α-helical segments within the range of 0–25° to the sixfold axis may not be uniquely diagnosed from the angular width of the equatorial arc. Interference effects do not, however, obscure the information in the diffraction fringes about the location and size of the transmembrane α-helical domain.

REFERENCES

Astbury, W. T., and A. Street. 1931. X-Ray studies of the structure of hair, wool, and related fibres. *Philos. Trans. R. Soc. Lond. A Math. Phys. Sci.* 230:75–101.

Banner, D. W., A. C. Bloomer, G. A. Petsko, D. C. Phillips, and I. A. Wilson. 1976. Atomic coordinates for triose phosphate isomerase from chicken muscle. *Biochem. Biophys. Res. Commun.* 72:146–155.

Bernstein, F. C., T. F. Koetzle, G. J. B. Williams, E. F. Meyer, M. D. Brice, J. R. Rodgers, O. Kennard, T. Schimanouchi, and M. Tasumi. 1977. The protein data bank: a computer-based archival file for macromolecular structure *J. Mol. Biol.* 112:535–542.

Beyer, E. C., D. L. Paul, and D. A. Goodenough. 1987. Connexin 43: a protein from rat heart homologous to a gap junction protein from liver. *J. Cell Biol.* 105:2621–2629.

Bolton, W., and M. F. Perutz. 1970. Three dimensional Fourier synthesis of horse deoxyhaemoglobin at 2.8 Å resolution. *Nature (Lond.)* 228:551–552.

Cantor, C. R., and P. R. Schimmel. 1980. Biophysical Chemistry. Part II. W. H. Freeman and Co., San Francisco, CA 409–480.

Caspar, D. L. D., D. A. Goodenough, L. Makowski, and W. C. Phillips. 1977. Gap junction structures I. Correlated electron microscopy and x-ray diffraction. *J. Cell Biol.* 74:605–628.

Caspar, D. L. D., G. E. Sosinsky, T. T. Tibbitts, W. C. Phillips, and D. A. Goodenough. 1988. Gap junction structure. *In* Gap Junctions. E. L. Hertzberg and R. Johnson, editors. Alan R. Liss, Inc., New York. 117–133.

Champness, J. N., A. C. Bloomer, G. Bricogne, P. J. G. Butler, and A. Klug. 1976. The structure of the protein disk of tobacco mosaic virus to 5 Å resolution *Nature (Lond.)*. 259:20–24

Chothia, C. 1975. Structural invariants in protein folding. *Nature (Lond)*. 254:304–308.

Fallon, R. F., and D. A. Goodenough. 1981. Five-hour half-life of mouse liver gap junction protein. *J. Cell Biol.* 90:521–526.

Finzel, B. C., P. C. Weber, K. D. Hardman, and F. R. Salemme. 1985. Structure of ferricytochrome *c'* from *Rhodospirillum molischianum* at 1.67 Å resolution. *J. Mol. Biol.* 186:627–643.

Fraser, R. D. B., T. P. MacRae, A. Miller, and R. J. Rowlands. 1976. Digital processing of fibre diffraction patterns. *J. Appl. Cryst.* 9:81–94.

Gimlich, R. L., N. M. Kumar, and N. B. Gilula. 1988. Sequence and developmental expression of mRNA coding for a gap junction protein in *Xenopus*. *J. Cell Biol.* 107:1056–1073.

Goodenough, D. A., D. L. Paul, and L. Jesaitis. 1988. Topological distribution of two connexin 32 antigenic sites in intact and split rodent hepatocyte gap junctions. *J. Cell Biol.* 107:1817–1824.

Guss, J. M., P. R. Harrowell, M. Murata, V. A. Norris, and H. C. Freeman. 1986. Crystal structure analyses of reduced (Cu^{I}) poplar plastocyanin at six pH values. *J. Mol. Biol.* 192:361–387.

Henderson, R. 1975. The structure of the purple membrane from *Halobacterium halobium:* analysis of the x-ray diffraction pattern. *J. Mol. Biol.* 93:123–138.

Henderson, R., and P. N. T. Unwin. 1975. Three-dimensional model of purple membrane obtained by electron microscopy. *Nature (Lond.).* 257:28–32.

Hertzberg, E. L., D. C. Spray, and R. Cook. 1988. Biochemical, immunological, and topological studies of gap junctions. *In* Gap Junctions. E. L. Hertzberg and R. Johnson, editors. Alan R. Liss, Inc., New York. 9–28.

Hopper, P., S. C. Harrison, and R. T. Sauer. 1984. Structure of tomato bushy stunt virus. V. Coat protein sequence determination and its structural implications. *J. Mol. Biol.* 177:701–713.

Jones, T. A. 1978. A graphics model building and refinement system for macromolecules. *J. Appl. Crystallogr.* 11:268–272.

Kumar, N. M., and H. B. Gilula. 1986. Cloning and characterization of human and rat liver cDNAs coding for a gap junction protein. *J. Cell Biol.* 103:767–776.

Makowski, L. 1985. Structural domains in gap junctions: implications for the control of intercellular communications. *In* Gap Junctions. M. V. L. Bennett and D. C. Spray, editors. Cold Spring Harbor Laboratories, New York. 5–12.

Makowski, L., D. L. D. Caspar, W. C. Phillips, and D. A. Goodenough. 1977. Gap junction structures. II. Analysis of the x-ray diffraction data. *J. Cell Biol.* 74:629–645.

Makowski, L., D. L. D. Caspar, and D. A. Marvin. 1980. Filamentous bacteriophage pf1 structure determined at 7 Å resolution by refinement of models for the α-helical subunit. *J. Mol. Biol.* 140:149–181.

Makowski, L., D. L. D. Caspar, D. A. Goodenough, and W. C. Phillips. 1982. Gap junction structures. III. The effect of variations in the isolation procedure. *Biophys. J.* 37:189–191.

Makowski, L., D. L. D. Caspar, W. C. Phillips, T. S. Baker, and D. A. Goodenough. 1984*a*. Gap junction structures. VI. Variation and conservation in connexon conformation and packing. *Biophys. J.* 45:208–218.

Makowski, L., D. L. D. Caspar, W. C. Phillips, and D. A. Goodenough. 1984*b*. Gap junction structures. V. Structural chemistry inferred from x-ray diffraction measurements on sucrose accessibility and trypsin susceptibility. *J. Mol. Bio.* 174:449–481.

Marvin, D. A. 1966. X-Ray diffraction and electron microscope studies on the structure of the small filamentous bacteriophage fd. *J. Mol. Biol.* 15:8–17.

Marvin, D. A., C. Nave, J. E. Ladner, A. G. Fowler, R. S. Brown, and E. J. Wachtel. 1981. Macromolecular structure transitions in pf1 filamentous bacterial virus. *In* Structural Aspects of Recognition and Assembly in Biological Macromolecules. Vol. 2. M. Balabain, J. L. Sussman, W. Traub, and A. Yonath, editors. Balaban ISS, Rehovot, Israel. 891–910.

Milks, L. C., N. M. Kumar, R. Houghten, N. Unwin, and N. B. Gilula. 1988. Topology of the 32-kd liver gap junction protein determined by site-directed antibody localizations. *EMBO (Eur. Mol. Biol. Organ.) J.* 7:2967–2975.

Mitsui, Y., Y. Satow, Y. Watanabe, and Y. Iitaka. 1979. Crystal structure of a bacterial protein proteinase inhibitor (*Streptomyces* subtilisin inhibitor) at 2.6 Å resolution. *J. Mol. Biol.* 131:697–724.

Musick, W. D. L., and M. G. Rossmann. 1979. The structure of mouse testicular lactate dehydrogenase isoenzyme C_4 at 2.9 Å resolution. *J. Biol. Chem.* 254:7611–7620.

Namba, K., and G. Stubbs. 1986. Structure of tobacco mosaic virus at 3.6 Å resolution. *Science (Wash. DC).* 231:1401–1406.

Paul, D. L. 1986. Molecular cloning of cDNA for rat liver gap junction protein. *J. Cell Biol.* 103:123–134.

Pauling, L., and R. B. Corey. 1951*a*. Atomic coordinates and structure factors for two helical configurations of polypeptide chains. *Proc. Natl. Acad Sci. USA.* 37:235–240.

Pauling, L., and R. B. Corey, 1951*b*. The pleated sheet, a new layer configuration of polypeptide chains. *Proc. Natl. Acad. Sci. USA.* 37:251–256.

Rees, D. C., M. Lewis, and W. N. Lipscomb. 1983. Refined crystal structure of carboxypeptidase A at 1.54 Å resolution. *J. Mol. Biol.* 168:367–387.

Richards, F. M. 1974. The interpretation of protein stuctures: total volume, group volume distributions and packing density. *J. Mol. Biol.* 82:1–14.

Richardson, J. S. 1981. The anatomy and taxonomy of protein structure. *Adv. Protein Chem.* 34:167–339.

Richardson, J. S., and D. C. Richardson. 1985. Interpretation of electron density maps. *Methods Enzymol.* 115:189–206.

Riley, D. P., and U. W. Arndt. 1953. X-Ray scattering by some native and denatured proteins in the solid state. *Proc. R. Soc. Lond. B Biol. Sci.* 141:93–97.

Sosinsky, G. E., J. C. Jésior, D. L. D. Caspar, and D. A. Goodenough. 1988. Gap Junction Structures VIII. Membrane cross-sections. *Biophys. J.* 53:709–722.

Smith, W. W., R. M. Burnett, G. D. Darling, and M. L. Ludwig. 1977. Structure of the semiquinone form of flavodoxin from *Clostridium* MP. Extension of 1.8 Å resolution and some comparisons with the oxidized state. *J. Mol. Biol.* 117:195–225.

Tibbitts, T. T., D. L. D. Caspar, W. Phillips, and D. Goodenough. 1988. Iterative convolution analysis of gap junction x-ray diffraction data. *Biophys. J.* 53:634a. (Abstr.)

Unwin, N. 1986. Is there a common design for cell membrane channels? *Nature (Lond.).* 323:12–13.

Unwin, P. N. T., and P. D. Ennis. 1984. Two configurations of a channel-forming membrane protein. *Nature (Lond.)* 307:609–613.

Unwin, P. N. T., and G. Zampighi. 1980. Structure of the junction between communicating cells. *Nature (Lond.).* 283:545–549.

Wilson, I. A., J. J. Skehel, and D. C. Wiley. 1981. Structure of the haemagglutinin membrane glycoprotein of influenza virus at 3 Å resolution. *Nature (Lond.)* 289:366–373.

Xu, Z.-B., and M. Schiffer. 1988. The refinement and structure of Mcg Bence-Jones dimer at 2.3 Å resolution. *Annu. Meeting Am. Crystallogr. Assoc.* 16:74. (Abstr.)